

Study of pulsed laser ablation products by optical probing

© M.I. Kulish,¹ A.V. Karabulin,^{1,2} V.I. Matyushenko^{1,3}

¹ Federal Research Center for Problems of Chemical Physics and Medical Chemistry, Russian Academy of Sciences, 142432 Chernogolovka, Moscow region, Russia

² Joint Institute for High Temperatures, Russian Academy of Sciences, 125412 Moscow, Russia

³ Chernogolovka Branch of the N.N. Semenov Federal Research Center for Chemical Physics, Russian Academy of Sciences, 142432 Chernogolovka, Moscow region, Russia
e-mail: avkarabulin@gmail.com

Received October 10, 2024

Revised August 8, 2025

Accepted September 25, 2025

A method for investigating products of pulsed laser ablation by measuring the absorption and scattering of light by small particles described by Mie theory is proposed. The method enabled obtaining data on the expansion velocity of the products, as well as estimating the amount of material evaporated per pulse.

Keywords: Mie scattering detection, pulsed laser ablation, optical probing, product expansion velocity.

DOI: 10.61011/TP.2026.01.62855.326-24

Introduction

Laser ablation is widely applied in various fields of science and technology: metal cutting and welding [1,2], ceramic processing [3], affecting surfaces of materials in order to change their properties [4], vision correction [5], etc. Recently, it is especially interesting to use pulsed laser ablation for producing nanomaterials, since it has a number of advantages as compared to chemical methods: relative simplicity and universality, which enables producing nanoparticles almost from any materials and, probably, the most important is purity of the produced nanomaterials [6].

Laser ablation in itself is a very complex multi-stage process that depends on multiple parameters: a laser used (duration and power of a pulse, an energy density, a wavelength, etc.), an ablated material (a substance, a surface condition), a medium in which it is ablated (vacuum, gas, liquid). More than 30 various models and mechanisms were proposed for describing such a complex phenomenon [7]. Nevertheless, the main method of obtaining information about a process and products of ablation is still an experiment.

It is known that during ablation of the materials with nanosecond and subnanosecond laser pulses there is simultaneously target evaporation and formation of a plasma torch, which result in formation of a target material vapor cloud with further formation of microparticles and nanoparticles [8]. In some practical applications, it is important to know time parameters of various stages of the process, including velocities of dispersion of various components and, as a whole, a configuration of the ablation torch [9]. An emerging plasma can shield a part of the pulse or subsequent pulses, sharply reducing ablation efficiency. The subsequent pulses can also affect the formed nanoparticles, resulting in undesirable variation of their properties.

The main way of investigating the ablation products includes various methods of electron microscopy. The very ablation process (interaction of the radiation pulse with the substance, the various stages of ablation product dispersion) is most often investigated using high-speed photo- and video-shooting that is usually combined with a variety of the schlieren method [10]. These methods have a number of disadvantages. First of all, high-speed video cameras that have required time resolution are expensive; secondly, these methods are very suitable for investigating luminescent objects (a plasma, particles heated to several thousand kelvins), but are less suitable for objects that do not radiate in a visible range; thirdly, objects with a size of less than visible light wavelengths are poorly recorded.

Using a quite simple method of recording probing laser radiation, which has been previously applied for investigating dispersion of microparticles ejected from the free surface of the material when a shock wave hits it [11,12], in the present study we have investigated velocities of motion and a density of a number of particles produced during laser ablation of the various metal targets in air and vacuum.

1. Experimental setup description

A diagram of the experimental setup is shown in Fig. 1. The cuvette with sapphire windows of the diameter of 2.5 cm and the thickness of 2 mm was arranged on the mobile platform to be moved in a horizontal plane perpendicular to a direction of the probing beam with accuracy of $\pm 5 \mu\text{m}$ by means of a micrometer screw. The cuvette could be evacuated to pressure $P = 0.2 \text{ Pa}$.

A flat metal target was placed in the cuvette perpendicular to the beam of the ablating laser. The targets were manufactured using chemically pure metals with purity of at least 99.99%.

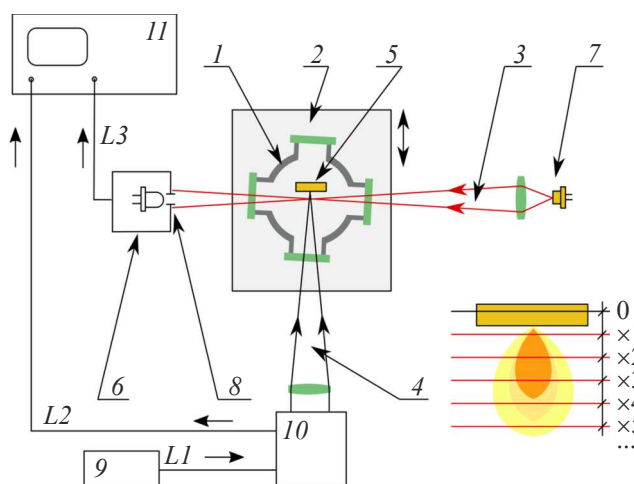


Figure 1. Optical diagram of the experiment (plan view): 1 — the optical cuvette, 2 — the mobile platform, 3 — the scanning laser beam, 4 — the ablating laser beam, 5 — the target, 6 — the photodiode, 7 — the laser diode, 8 — the diaphragm, 9 — the generator, 10 — the pulse laser, 11 — the oscilloscope Tektronix 5054; L1 — the pulse laser activation line L2 — the line for triggering the oscilloscope when the pulse laser is actuated; L3 — the line for supplying a detector signal to the oscilloscope. To the right below is a conventional diagram of relative arrangement of the target and the probing beam, a coordinate X of the beam position was counted not from a target surface, but from an initial position „0“ near the target surface.

The targets were ablated using a laser with the following parameters: the wavelength $\lambda = 1064$ nm, pulse duration $\tau_p = 0.6$ ns, pulse energy $E_p = 0.1$ mJ, a repetition rate was up to 4 kHz. Laser radiation was focused to the target surface by means of a lens with a focal distance of 28 cm into a spot of the diameter of $100 \mu\text{m}$. A radiation power density of the ablating laser in the focal spot was ~ 3.6 GW/cm². In order to avoid burn through of the target when a signal was recorded, the laser beam was moved along its surface parallel to the direction of the probing beam by means of a motorized adjuster at the velocity ~ 1 mm/min.

For probing, we have applied continuous radiation of the laser diode with the wavelength of 660 nm and maximum radiation power of 120 mW. The radiation power was adjusted by a diode current. Probing radiation was measured using the silicon photodiode SFH203 with sensitivity of 0.45 A/W at the wavelength of laser radiation and a signal increase time of at most 5 ns. A diaphragm of the diameter of 1 mm was placed in front of the photodiode. An oscilloscope trigger was actuated from a signal of synchronization of the ablating pulse laser. The laser diode's current was set up so that the detector signal did not exceed the value of 500 mV, which was safe for it in terms of scattered continuous power. At the same time, power of probing radiation at the photodetector did not exceed ~ 20 mW.

Probing laser radiation was focused by means of the lens within the area of the target into a waist, whose diameter was measured by means of a laser beam profile analyzer Beamage-3.0 manufactured by Standa. The effective value of the waist diameter in the thinnest place was $90 \mu\text{m}$, whereas a waist length, at which its diameter varies by at most 10% was about 1 cm.

Prior to start of the measurements, the target was brought to a probing beam axis before start of reduction of the photodiode signal due to partial overlapping of the beam by the target. It was followed by removing the target into the initial position, in which the signal was up to 100%, and performing a series of measurements in a number of increasing distances from the target to the probing beam axis (the range of variation of the distances was about 1 mm).

When passing through an area that has ablation products, the scanning beam is attenuated due to scattering and absorption on the particles. A value of this attenuation can be used to determine a number of scattering particles.

The products generated during ablation settled to a cell bottom, which included standard copper meshes that are coated by a perforated carbon film and usually used in transmission electron microscopy. Then the samples were studied in an electron microscope JEOL JEM-2100.

2. Results and discussion

The typical oscillogram for the experiment with the tungsten target in air is shown in Fig. 2. One can select several typical areas that are designated by digits in the figure, which will be considered in detail below.

At the initial moment of time, which coincides with the ablating laser pulse, intensity of transmitted radiation of the probing laser I at all the distances to the target is equal to I_0 , which is initial intensity, thereby indicating that the area of

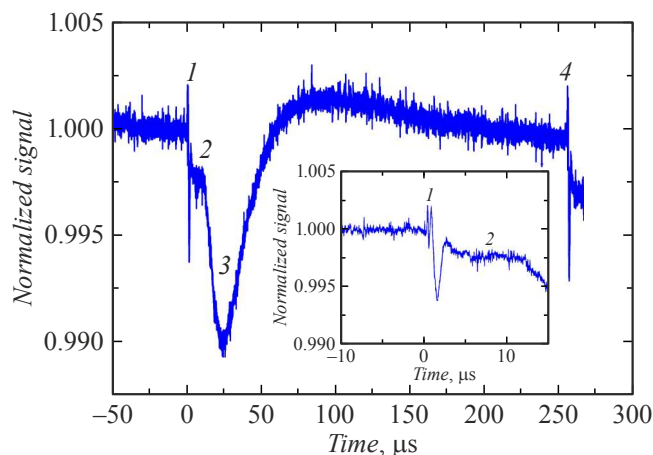


Figure 2. Normalized signal for the target position $X = 680$. 1 — beam diffraction at the leading front, 2 — a „fast“ maximum of absorption, 3 — „a slow“ maximum of absorption, 4 — the next laser pulse. The insert shows the initial area of the signal.

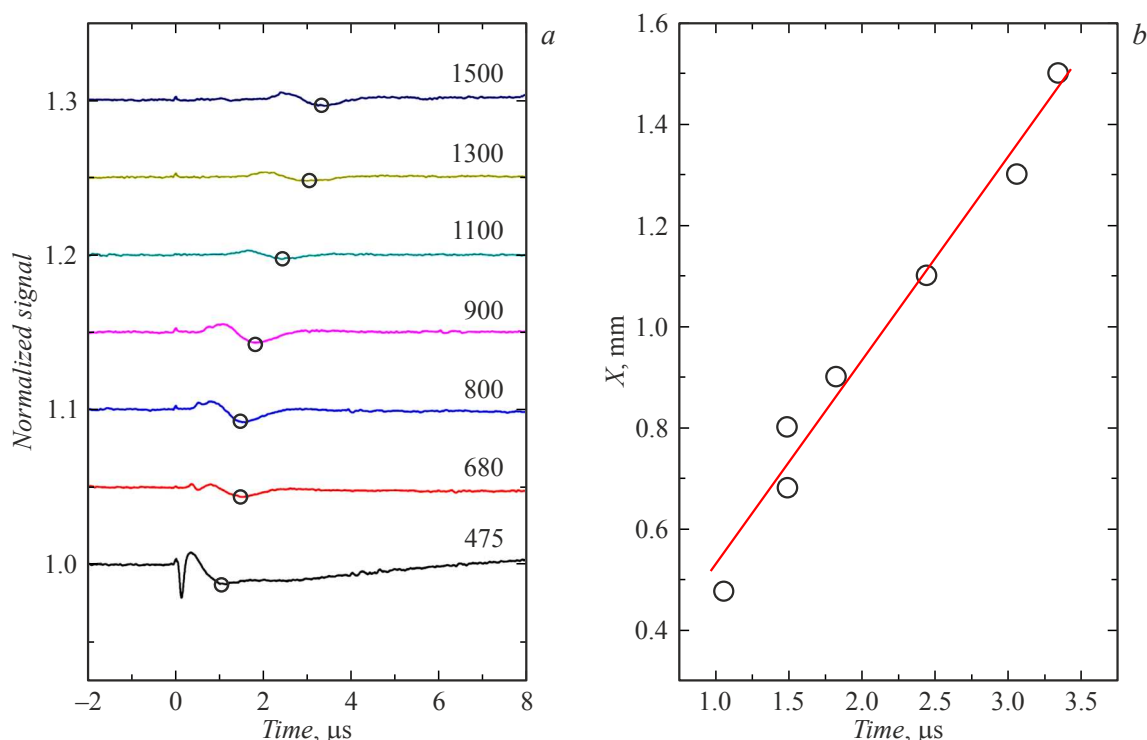


Figure 3. Oscillograms of the normalized experimental signals in a dependence on the coordinate X for the „fast“ maximum of signal absorption. On the right is shown a $x - t$ trajectory of the „fast“ maximum of absorption 2.

the probing beam has not optical heterogeneities that could result in its scattering or absorption.

In several tenths of a microsecond, the initial portion I exhibits oscillations caused by Fresnel diffraction, wherein intensity of recorded radiation can exceed the initial one ($I > I_0$). The literature deals with this effect in detail when observing coverage of stars by the Moon [13], but it can also be caused by a density surge either in the shockwave [14,15] during dispersion of the products in the air atmosphere or in a leading part of the substance flow during dispersion in vacuum.

After it, initial absorption is observed ($I < I_0$) — the portion 2. This reduction of intensity is related to the fact that a part of probing radiation is scattered or absorbed on the laser ablation products. Fig. 3, *a* shows oscillograms of the signals taken at the various distances from the target. The value of X in Fig. 2–4 is readings of the micrometer screw, wherein $X = 475$ corresponds to a scanning beam position that is nearest to the target. For clarity, the normalized signals are subsequently shifted along the vertical by the value of 0.05. Circles mark positions of the portions 2. In order to calculate the velocity, points were marked in the coordinates $X - t$, where X is a position of the probing beam axis and t is time of the maximum of radiation absorption for this X . The least-square method was used to determine a slope of a straight line, which in the best way approximated the dependence of X on time. A random error of the value of the velocity is $\sim \pm 10$ m/s. The slope of the straight line on the $x - t$ diagram in Fig. 3, *b*

corresponds to motion of the leading front of the tungsten ablation products in the air atmosphere at the velocity ~ 450 m/s. When removing the probing beam from the target surface, the typical portions of the signal shown in Fig. 2, are extended along the time axis and the portions 2 and 3 more and more lag behind the portion 1.

In addition to initial absorption (the portion 2), one can clearly see an absorption peak that designated in Fig. 2 by the digit 3. Oscillograms for this portion are shown in Fig. 4, *a*. It is clear from the $x - t$ diagram in Fig. 4, *b* that the velocity that is determined by a given procedure and belongs to the maximum of absorption of probing radiation is ~ 4 m/s for the portion 3. For the slow component, in which the velocity depends on time, the dependence X on time was approximated by a second-power polynomial. The low value of the velocity, which is recorded by delay of the maximum of absorption, reflects slow variation of the absorption coefficient in the area that belongs to a rear part of the flow.

It should be noted that the portion 3 is absent in vacuum — after the portion with a fast component of absorption intensity of the probing beam returns to the initial value I_0 . This and a very slow velocity of propagation and duration of the process that is up to several tens of microseconds cause certain difficulties in interpreting the data obtained. The authors know only one study that has investigated ablation into air of atmospheric pressure at quite long times [16]. It is shown in it that higher pressure in the graphite ablation torch expels surrounding air and for at

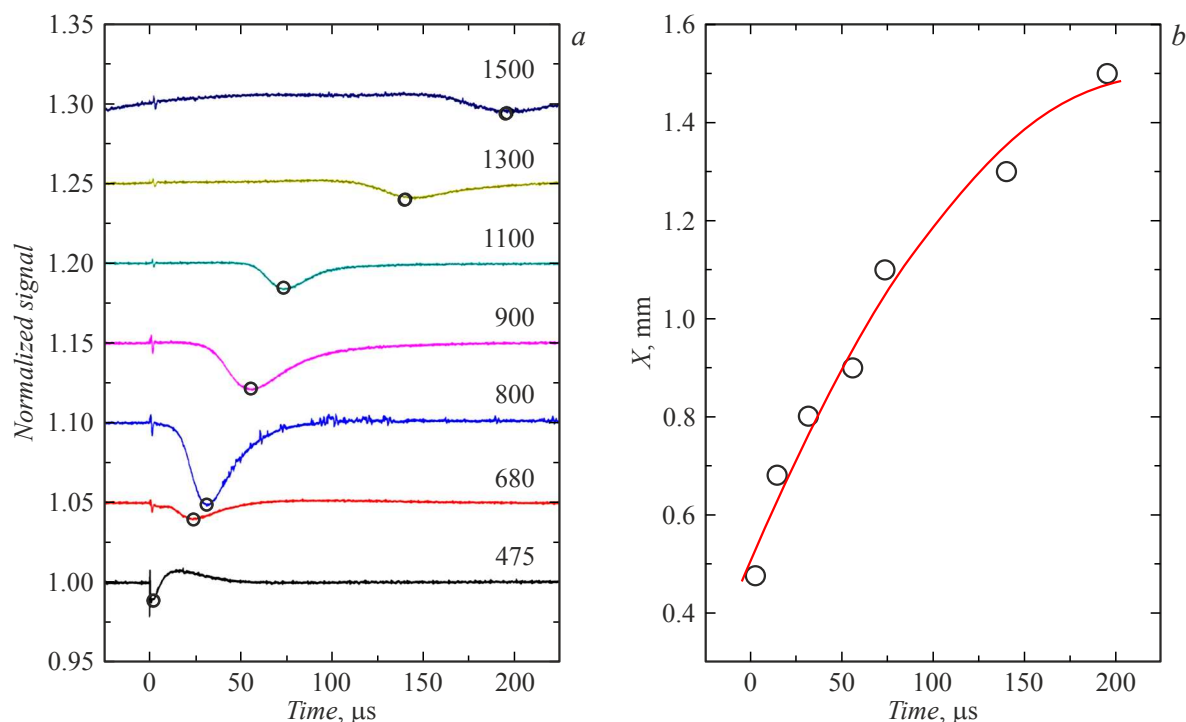


Figure 4. Oscillograms of the normalized experimental signals in a dependence on the coordinate X . On the right is shown a $x - t$ trajectory of the „slow“ maximum of absorption 3.

least several tens of microseconds there is an area that exists near the target and is filled only by the ablation products. It can be assumed that the similar scenario is realized in our case. There is a cloud of the ablation products, which is formed near the target and effectively absorbs and scattered the scanning beam. This cloud slowly drifts from the target as a whole unit.

Finally, to the moment of arrival of the next pulse (the digit 4 in Fig. 2), intensity of the scanning beam I again becomes equal to the initial one I_0 .

Table shows the obtained particle dispersion velocities for the various metals in air at 1 atm and in vacuum for tungsten. The velocities V_1 and V_2 are velocities of motion of the particles for a „fast“ (the portion 2) and a „slow“ shift of the maximums of absorption of probing radiation (the portion 3). It is clear that the velocities V_1 for the various metals turned out to be approximately the same and are

~ 450 m/s. The velocities obtained in our experiments are close to those observed for the ablation torch that expands in a gas and predominantly consists of neutral atoms and clusters [17].

The experiment with tungsten in vacuum (0.2 Pa) was performed with continuous evacuation of the cell. The velocity of the „fast“ shift of the maximum of absorption was somewhat higher than in vacuum and was ~ 600 m/s. The „slow“ maximum was not observed during ablation in vacuum.

In addition to determining the product dispersion velocities, the procedure makes it possible to estimate some other ablation parameters as well, for example, a substance weight evaporated by a single pulse and an average number of particles in a volume at the various distances from the target. We exemplify it by tungsten.

In order to estimate intensity of transmitted radiation I with radiation intensity before the target I_0 , the following expression can be applied

$$I = I_0 \cdot e^{-\tau w}, \tag{1}$$

where w is a length of the absorbing layer, which is equal to an effective diameter of the ablation flow, in which the probing beam $\approx 100 \mu\text{m}$, and τ — the absorption coefficient.

The absorption coefficient τ can be written [11] as

$$\tau = \int_0^\infty N f(r) q_{\text{ext}}(r) \pi r^2 dr = N \int_0^\infty q_{\text{ext}} \pi r^2 f(r) dr = NS. \tag{2}$$

Velocities of dispersion of the particles of the various metals

Metal	Ni	W	Sn	Re
Air, atmospheric pressure				
Velocity V_1 , m/s	470	440	420	350
Velocity V_2 , m/s	4.5	4.4	3.5 – 7.3	5.9
Vacuum, 0.2 Pa				
Velocity V_1 , m/s		≈ 600		

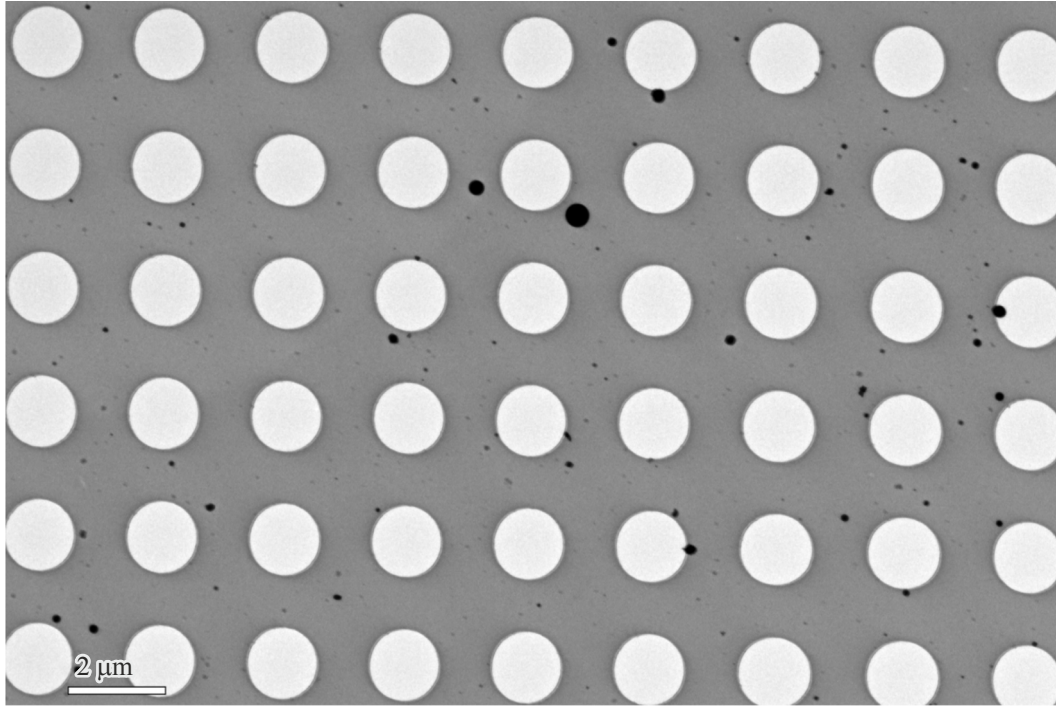


Figure 5. TEM image of the ablation products of the tungsten target.

Here N is a full number of particles in a unit volume, q_{ext} is an extinction coefficient of a spherical particle, and S is an absorption cross-section per one particle on average.

The formula (1) can be rewritten as

$$\tau = 1/w \ln\left(\frac{I_0}{I}\right). \quad (3)$$

A ratio of the transmitted part of radiation to the initial one is $I/I_0 = 0.9987$ for the portion 2 (Fig. 2).

Further calculations require to pre-define a function of size distribution of particles $f(r)$. As a rule, the laser ablation products are spherical clusters, whose size distribution is usually described by a lognormal function and the sizes vary from several to hundred nanometers [18]:

$$f(r) = \frac{1}{r\sigma\sqrt{2\pi}} \exp\left(\frac{-\left(\ln\left(\frac{r}{m}\right)\right)^2}{2\sigma^2}\right). \quad (4)$$

In order to determine the coefficients σ and m , the Fiji software package was used to analyze the TEM images of the products of laser ablation of the tungsten target in air, which settled to the TEM mesh (Fig. 5) in an assumption that the size distribution of the settled particles is not much different from that in the probing area.

The size distribution of particles was analyzed to provide the values of the coefficients $\sigma = 1.226$ and $m = 0.02023$ at a value of the particle radius r , which is measured in micrometers. The average particle diameter was 75 nm.

The distribution function $f(r)$ satisfies the normalization condition

$$\int_0^{\infty} f(r)dr = 1.$$

Absorption of light by a medium with volume-distributed spherical particles was calculated using the Mie scattering theory. The extinction coefficient of the spherical tungsten particles in a dependence on the size is calculated in an online calculator [19] with data of tungsten optical constants from the study [20]. It was calculated for a complex refractive index: $\varepsilon = n + ik$ when $n = 0.91625$ and $k = 7.0381$.

After determining the extinction coefficient and the size distribution of particles, we can calculate an absorption cross-section per one particle on average:

$$S = \int_0^{\infty} q_{\text{ext}} \pi r^2 f(r)dr.$$

The magnitude $S = 0.06 \mu\text{m}^2$.

Thus, experimentally determining τ and calculating S , we can find a number of particles in the studied area.

The number of particles in the probing laser beam for the coordinates $X = 475$ and 680 is shown in Fig. 6.

In the position $X = 475$ that corresponds to the configuration, in which all the ejected particles are transmitted through the scanning beam almost touching the target surface, the present procedure allows determining the total substance weight ablated per pulse. When removing the probing beam from the target, for example, in the position $X = 680$, the volume occupied by particles increases, the

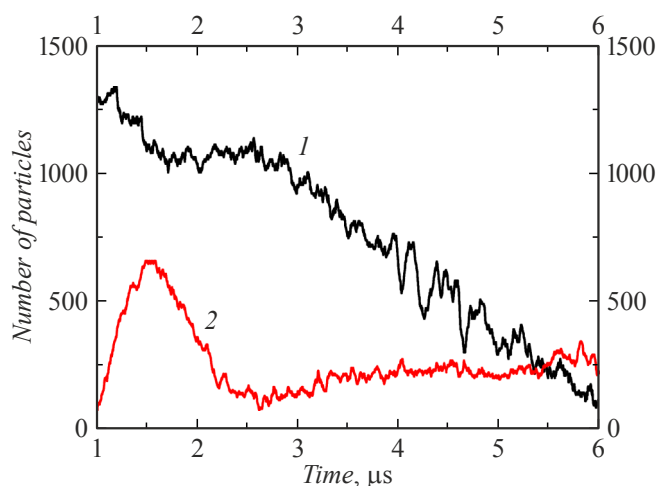


Figure 6. Number of particles absorbing radiation of the probing laser for the two coordinates of the probing beam X : 1 — 475, 2 — 680.

number of particles in the unit volume decreases and absorption decreases in the flat portion 2 (Fig. 2). In this case, additional data on the shape of the ablation torch are required to determine the total number of nanoparticles. The maximum of the number of particles on the curve 2 corresponds to the „fast“ maximum of absorption of the signal.

After amplitude oscillations related to diffraction of the probing beam at the leading front of the flow, starting from $\sim 1 \mu\text{s}$, the number of recorded particles in the cylinder of the diameter of $90 \mu\text{m}$ and the height of about $100 \mu\text{m}$ goes to the plateau and then starts decreasing to reach zero around $6 \mu\text{s}$. It can be assumed that within this time all the particles formed after the laser pulse fly through. Integration of the signal within the range $1 - 6 \mu\text{s}$ provides the total number of the ejected particles. On average, about 15 000 particles of the average diameter of 75 nm are formed per one pulse. Knowing the tungsten density $\rho = 19.25 \text{ g/cm}^3$, one can estimate the weight ablated by one laser pulse: it is about 0.065 ng . In order to estimate our obtained value, we used a precision balance Mettler Toledo ME204T/A00 (precision is 0.1 mg) to weigh the tungsten target before and after ablation for 60 min with a pulse rate of 4000 Hz . The target weight decreased by $(1.8 \pm 0.1) \text{ mg}$, or by 0.13 ng per pulse. It can be stated that the procedure proposed in the present study makes it possible to quite accurately estimate a substance weight ejected per pulse in the form of nano- and micro-particles.

Conclusion

The products of pulsed laser ablation of the various metal targets have been studied in air under the normal conditions and in vacuum by the method of measuring absorption and scattering of probing optical radiation. Transmittance of light

by the medium with volume-distributed spherical particles was calculated using the Mie theory. We have determined the velocities of dispersion of particles of nickel, tungsten, tin, rhenium in air and particles of tungsten in vacuum (0.2 Pa). We have determined the weight of the substance ablated per one pulse.

Funding

The study has been performed according to topics of the state assignments №124020600049-8, №075-00269-25-00 and №125012200612-2.

Conflict of interest

The authors declare that they have no conflict of interest.

References

- [1] S. Pak, Y. Kim, K.Y. Park, K.D. Lee, M.S. Cheon, H.G. Lee. *Fusion Eng. Design*, **85**, 190 (2010). DOI: 10.1016/j.fusengdes.2009.11.003
- [2] A. Sharma, V. Yadava. *Opt. Laser Technol.*, **98**, 264 (2018). DOI: 10.1016/j.optlastec.2017.08.002
- [3] H.-J. Wang. *J. Europ. Ceramic Society*, **41**, 4997 (2021). DOI: 10.1016/j.jeurceramsoc.2021.04.019
- [4] C.R. Phipps (ed.). *Laser ablation and its applications* (Springer, NY., 2007)
- [5] G.L. Ehlke. *Asia-Pacific J. Ophthalmology*, **5**, 434 (2016). DOI: 10.1097/APO.0000000000000237
- [6] A. Hahn, S. Barcikowski, B. Chichkov. *J. Laser Micro/Nanoengineering*, **3**, 73 (2008). DOI: 10.2961/jlmn.2008.02.0003
- [7] R.E. Russo. *Appl. Phys. A*, **129**, 168 (2023). DOI: 10.1007/s00339-023-06425-3.
- [8] A. Kanitz, M.-R. Kalus, E.L. Gurevich, A. Ostendorf, S. Barcikowski, D. Amans. *Plasma Sources Sci. Technol.*, **28**, 103001 (2019). DOI: 10.1088/1361-6595/ab3dbe.
- [9] C. Dowding. *Laser ablation. In Advances in Laser Materials Processing* (Elsevier, 2010), p. 575–628. DOI: 10.1533/9781845699819.7.575
- [10] W. Soliman, N. Takada, K. Sasaki. *Appl. Phys. Express*, **3**, 035201 (2010). DOI: 10.1143/APEX.3.035201
- [11] S.K. Monfared, W.T. Buttler, D.K. Frayer, M. Grover, B.M. LaLone, G.D. Stevens, J.B. Stone, W.D. Turley, M.M. Schauer. *J. Appl. Phys.*, **117**, 223105 (2015). DOI: 10.1063/1.4922180
- [12] M.I. Kulish, S.V. Dudin, A.E. Ushnurtsev, V.B. Mintsev. *J. Phys.: Conf. Ser.*, **1556**, 012023 (2020). DOI: 10.1088/1742-6596/1556/1/012023
- [13] A. Malawi. *Lunar Occultation*. In Y.H. Chemin (ed.), *Lunar Science* (Intech. Open, 2019), DOI: 10.5772/intechopen.86110
- [14] G.R. Cowan, D.F. Hornig. *J. Chem. Phys.*, **18**, 1008 (1950). DOI: 10.1063/1.1747845
- [15] I. Mursenkova, M. Timokhin, M. Tikhonov, A. Militsina, A. Kuznetsov. *J. Phys.: Conf. Ser.*, **2127**, 012001 (2021). DOI: 10.1088/1742-6596/2127/1/012001
- [16] A.M. Ojeda, C.W. Schneider, T. Lippert, A. Wokaun. *J. Appl. Phys.*, **120**, 225301 (2016). DOI: 10.1063/1.4971251

- [17] K. Sasaki, H. Watarai. Jpn. J. Appl. Phys., **45** (4L), L447 (2006). DOI: 10.1143/JJAP.45.L447
- [18] N.G. Semaltianos. Critical Rev. Solid State Mater. Sci., **35**, 105 (2010). DOI: 10.1080/10408431003788233
- [19] Electronic source. *Mie calculator: New Phystech. ITMO University*. Available at:
<https://physics.itmo.ru/ru/mie#/spectrum>
- [20] W.S.M. Werner, K. Glantschnig, C. Ambrosch-Draxl. J. Phys. Chem. Ref. Data, **38**, 1013 (2009). DOI: 10.1063/1.3243762

Translated by M.Shevelev